NEXAFS and XMCD studies of single-phase Co doped ZnO thin films

2009 J. Phys.: Condens. Matter 21 185005

(http://iopscience.iop.org/0953-8984/21/18/185005)

J. Phys.: Condens. Matter **21** (2009) 185005 (7pp) doi:10.1088/0953-8984/21/18/185005

NEXAFS and XMCD studies of single-phase Co doped ZnO thin films

Abhinav Pratap Singh[1], Ravi Kumar[1], P Thakur[2], N B Brookes[2], K H Chae[3] and W K Choi[3]

[1] Materials Science Division, Inter University Accelerator Centre, Aruna Asaf Ali Marg, New Delhi 110067, India
[2] European Synchrotron Radiation Facility, BP220, 38043 Grenoble Cedex, France
[3] Materials Science and Technology Research Division, KIST, Seoul 136-791, Korea

E-mail: abhi.pr.s@gmail.com

Received 16 January 2009, in final form 3 February 2009
Published 11 March 2009
Online at stacks.iop.org/JPhysCM/21/185005

Abstract

A study of the electronic structure and magnetic properties of Co doped ZnO thin films synthesized by ion implantation followed by swift heavy ion irradiation is presented using near-edge x-ray absorption fine structure (NEXAFS) and x-ray magnetic circular dichroism (XMCD) measurements. The spectral features of NEXAFS at the Co $L_{3,2}$-edge show entirely different features than that of metallic Co clusters and other Co oxide phases. The atomic multiplet calculations are performed to determine the valence state, symmetry and the crystal field splitting, which show that in the present system Co is in the 2+ state and substituted at the Zn site in tetrahedral symmetry with $10Dq = -0.6$ eV. The ferromagnetic character of these materials is confirmed through XMCD spectra. To rule out the possibilities of defect induced magnetism, the results are compared with Ar annealed and Ar-ion implanted pure ZnO thin films. The presented results confirm the substitution of Co at the Zn site in the ZnO matrix, which is responsible for room temperature ferromagnetism.

1. Introduction

Transition metal doped ZnO based diluted magnetic semiconductor (DMS) systems are being extensively studied for various reasons. These are seen as the potential candidates for the source of spin polarized current in the field of spintronics, which can help in the realization of spintronics devices [1]. Apart from the application point of view, these systems are also presenting many challenges to our understanding of the nature of magnetism in these systems. Room temperature ferromagnetism (RTFM) is seen in these systems with very small concentration of transition metal doping. The Zener mean field model has predicted the possibility of ferromagnetism above room temperature in a semiconducting system [2], but there are reports of observation of RTFM in insulating systems as well [3]. Attempts have been made to explain these observations using the bound magnetic polaron (BMP) model [4]. But this model explains only certain features of the magnetism. It has also been claimed that the presence of defects may be responsible for ferromagnetism [5] and the transition metal ion doping is not required for the RTFM. There are reports on C doped ZnO [6] and Ar-ion implanted ZnO [7] systems exhibiting ferromagnetism. All these reports cast doubt about whether the transition metal doping or defects are responsible for the observed magnetism in ZnO.

One important issue that must be resolved before proposing these systems as the true DMS material is the presence/absence of the secondary phases/clusters of the doped transition metal ions. It is often observed that the magnetism is due to the clusters of transition metals or their oxide phases and is not intrinsic to the system. The near-edge x-ray absorption fine structure (NEXAFS) has proven to be a very effective experimental tool to understand such situations. It is an element specific technique, which can give information about the charge state, local environment, and hybridization etc of specific cations present in the material. On the other hand, x-ray magnetic circular dichroism (XMCD) can be used to obtain information regarding the contribution of a specific cation in any material towards the total magnetism of the system. It is also used to separate out the spin and orbital contributions to the magnetism using simple sum rules [8, 9]. Here we report the NEXAFS and XMCD studies of the Co doped

ZnO thin films prepared using ion implantation followed by swift heavy ion (SHI) irradiation. The as-implanted ZnO thin films were found to have impurity phases. To dissolve these phases, the films were irradiated with 200 MeV Ag^{15+}-ions. Various characterization techniques have been used to investigate the properties of the Co doped ZnO thin films, which suggest that the system is single phase and magnetism is due to the substitutional Co doping. These results are reported elsewhere [10, 11]. To further investigate the role played by the defects in the system, we also report the results of pure ZnO thin films (i) annealed in Ar environment at 500 °C for 2 h and (ii) implanted with 100 keV Ar-ions to produce a controlled number of O vacancies and the defects introduced into the system due to the ion implantation. The results are compared between Co doped ZnO and controlled defect generated pure ZnO thin films.

2. Experimental details

Thin films of ZnO of thickness ∼400 nm were deposited on α-Al_2O_3(0001) substrate using plasma-assisted molecular beam epitaxy (PAMBE). The substrate temperature during deposition was 720 °C and the chamber pressure was 2×10^{-9} Torr. The details of the film deposition can be found elsewhere [12]. The well characterized films were implanted using a source of negative ions by caesium sputtering (SNICS) with 80 keV Co ions at 300 °C to recover the implantation damage. The range of 80 keV Co ions in ZnO as calculated using SRIM2008 is 35.5 nm with a longitudinal straggling of around 16 nm. Thus all the Co ions are implanted in the ZnO film. The fluence for the ion implantation was 1×10^{16}, 2×10^{16}, 5×10^{16} and 1×10^{17} ions cm^{-2}. The implanted films were then irradiated with 200 MeV Ag^{15+}-ions with a fluence of 1×10^{12} ions cm^{-2} using the 15 UD tandem accelerator at the Inter University Accelerator Centre, New Delhi. From here onwards the films implanted with doses of 1×10^{16}, 2×10^{16}, 5×10^{16} and 1×10^{17} ions cm^{-2} followed by 200 MeV Ag^{15+}-ion irradiation will be named as CoZnO1, CoZnO2, CoZnO3, and CoZnO4 respectively. To study the defect induced magnetism, pure ZnO thin films were (i) annealed in Ar gas environment at 500 °C for 2 h and (ii) implanted with 100 keV Ar-ions with fluence of 1×10^{16}, 5×10^{16} and 1×10^{17} ions cm^{-2}, named as ArZnO1, ArZnO2 and ArZnO3, respectively.

High resolution x-ray diffraction was measured using a KM (6 + 2)-circle diffractometer in an 8Cl x-ray beamline of the Pohang light source (PLS) operated at 2.5 GeV in the energy range of 3–22 keV. The NEXAFS and XMCD experiments were carried out at the 2A MS beamline of the PLS and some parts of the measurements were repeated at the ESRF's ID08 beamline, which uses an APPLE II type undulator giving ∼100% linear/circular polarization. All scans were collected in total electron yield mode and the base pressure of the experimental chamber was better than 5×10^{-10} Torr. The XMCD spectra were taken for fixed helicity of the light by reversing the magnetic field (0.3 T) for each energy value of the incident x-ray photon. The spectra were normalized to incident photon flux. The magnetization measurements were performed at 300 K using an alternating gradient force magnetometer (AGFM) (micromag-2900, Princeton Measurements Co.) with a sensitivity of 10^{-8} emu.

3. Results and discussions

Figure 1 shows the x-ray diffraction pattern (XRD) of the as-implanted and then swift heavy ion (SHI) irradiated ZnO thin films. It is clear from figure 1 that the films are highly epitaxial with preferred orientation along the (001) direction. For the as-implanted samples, all the peaks have been indexed as ZnO or Al_2O_3 (substrate) peaks except for the impurity peak at around $2\theta = 44.3°$, indicated in figure 1 with an asterisk. This peak has been identified as the Co(111) peak. It can be seen from figure 1 that with the increase in implantation dose this peak ($2\theta = 44.3°$) is becoming sharp with increasing intensity. This may be due to the increase in size of the Co clusters with increase in implantation dose. Here only the representative samples with implantation dose of 5×10^{16} and 1×10^{17} ions cm^{-2} are presented. Similar trends were observed in other samples as well [10, 11]. To dissolve these Co clusters, the implanted samples were then irradiated with 200 MeV Ag^{15+}-ions with a fluence of 1×10^{12} ions cm^{-2}. After irradiation, it was found that the samples implanted with doses of 1×10^{16}, 2×10^{16} and 5×10^{16} ions cm^{-2} are single phase while the sample with implantation dose of 1×10^{17} ions cm^{-2} still contains the Co(111) impurity peak. So it is concluded that SHI irradiation has helped in dissolving the Co clusters that were present just after implantation in the case of CoZnO1, CoZnO2 and CoZnO3 samples. This is explained very well in the literature with the help of the thermal spike model [10, 11]. According to the thermal spike model, as the swift heavy ion (with energy in MeV) passes through the material it deposits its energy mainly via transferring its energy to electrons and then this energy is transferred to the lattice via electron–phonon coupling. This leads to rapid heating of the lattice with temperatures reaching far above the melting points of the materials involved. This rapid heating is localized around the travelling ion path in the material and is followed by a rapid thermal quenching (∼10^{13}–10^{14} K s^{-1}) [13]. Thus the thermal spike so produced is highly localized in both space and time. Hence when the SHI passes through the material, it makes a solid solution of ZnO and Co. The rapid thermal quenching, which follows this heating, does not allow Co to go to the interstitial site and Co substitutes for Zn in the ZnO matrix. When the 200 MeV Ag^{15+}-ion passes through the ZnO matrix, it produces an ion track of around 100 nm^2 cross-sectional area. Thus the number of ions required per cm^2 area will be 1 cm^2/100 nm^2 = 1×10^{12}. This explains the value of ion fluence used for SHI irradiation. For the film implanted with implantation dose of 1×10^{17} ions cm^{-2}, it is believed that the presence of Co clusters after irradiation is because of the fact that the amount of Co present in the system is beyond the solubility limit of Co in the ZnO matrix. From the above analysis it has been observed that the solubility limit of Co in the ZnO matrix is below 5%.

The samples exhibit room temperature ferromagnetism, which has been reported along with the detailed analysis

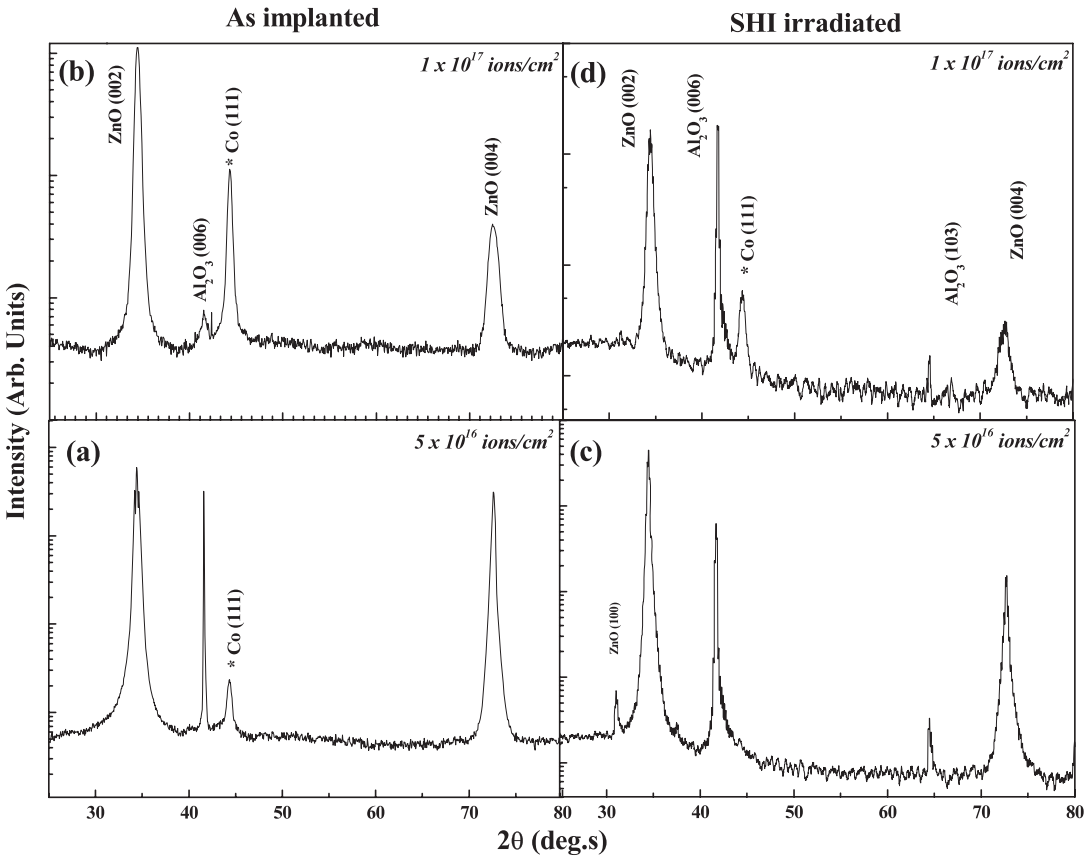

Figure 1. X-ray diffraction of the as-implanted Co doped samples and the 200 MeV Ag^{15+}-ion irradiated samples. The implantation doses are 5×10^{16} and 1×10^{17} ions cm^{-2}, and the irradiation dose is 1×10^{12} ions cm^{-2}.

elsewhere [10, 11]. There may be many controversies regarding the source of magnetism in these systems, such as the presence of Co clusters, defect states etc. To investigate the role of Co doping and to ascertain its position in the ZnO matrix, NEXAFS spectra were collected at the Co $L_{3,2}$-edge for the CoZnO1, CoZnO2, CoZnO3 and CoZnO4 samples. It is known that NEXAFS is an element-selective technique in which the spectral features are very much sensitive to the local environment or the symmetry of the probed ion. It can be a very effective tool to determine whether the Co is present as clusters or in any other oxide phase or whether it is substituting at the Zn site in the ZnO. Figure 2 shows the NEXAFS spectra at the Co $L_{3,2}$-edge at 300 K for the CoZnO1, CoZnO2, CoZnO3 and CoZnO4 samples along with Co_3O_4 as a reference compound. It can be seen from figure 2 that the spectral features of the CoZnO1, CoZnO2 and CoZnO3 samples are similar to each other but the spectral features of the CoZnO4 sample are completely different. The spectral features of the CoZnO4 sample are similar to those of the Co metal reported in the literature [14]. This further confirms the presence of Co clusters in the CoZnO4 sample in accordance with the XRD results. For the CoZnO1, CoZnO2 and CoZnO3 samples, the spectral features are neither similar to Co metal nor to Co_3O_4. The presence of the oxide phases of Co is also ruled out from the XRD results in which no peaks corresponding to any of the cobalt oxide phases were detected. Moreover, spectral features of the Co doped samples remain unchanged

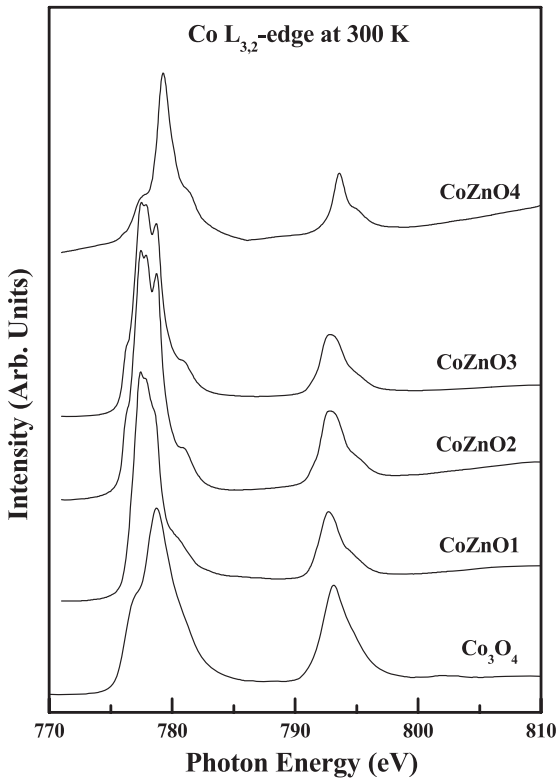

Figure 2. Near-edge x-ray absorption fine structure (NEXAFS) at the Co $L_{3,2}$-edge at 300 K of the Co doped ZnO samples and Co_3O_4.

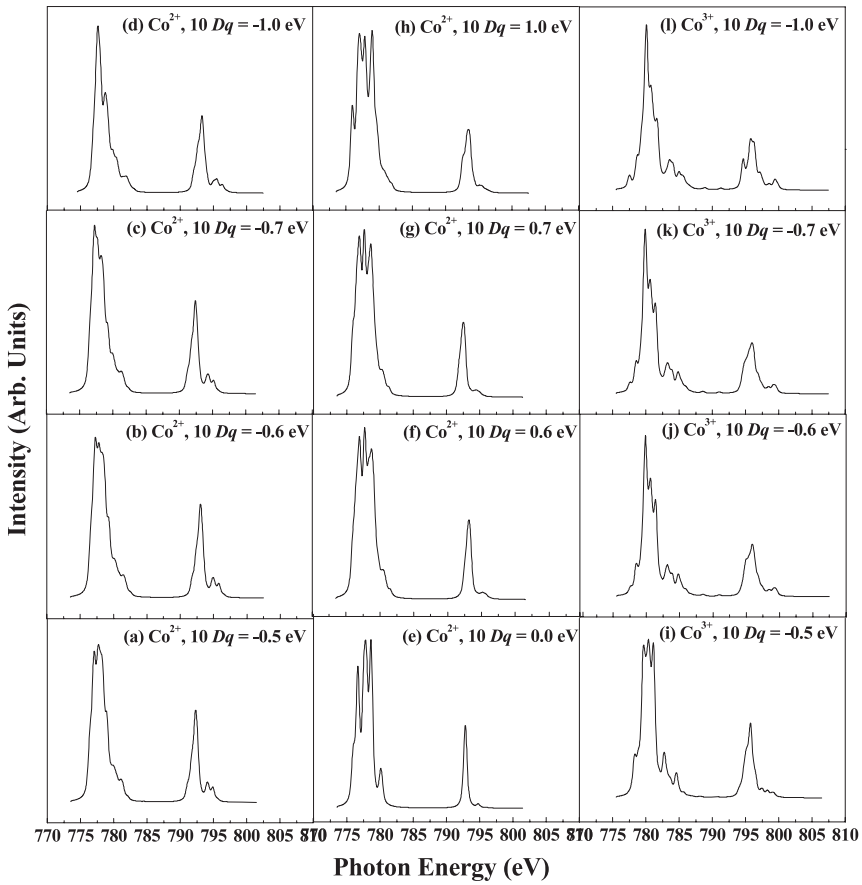

Figure 3. The calculated Co $L_{3,2}$-edge with various values of crystal field splitting ($10Dq$).

with temperature (not shown here) indicating that there is a negligible change in the surrounding of the Co ions with the change in temperature. To further understand about the local environment of the Co ions, atomic multiplet calculations were performed in various symmetries with different valence states of the Co ions at the Co $L_{3,2}$-edge. It was found that the spectral features were better reproduced with the Co in the 2+ state surrounded tetrahedrally by four O ions. Figure 3 shows results of these calculations with Co in the 2+ (figures 3(a)–(h)) and 3+ state (figures 3(i)–(l)). Values of the crystal field splitting ($10Dq$) used in the calculations are mentioned in each plot of figure 3. Here the positive values of $10Dq$ indicate the octahedral symmetry whereas the negative values effectively produce tetrahedral symmetry; a zero crystal field value means that the ion is in spherical symmetry. To compare the discrete lines of the atomic multiplets with the experiment, they have been broadened with a Lorentzian of 0.2 eV to simulate the lifetime broadening and convoluted with a Gaussian broadening of 0.15 eV to simulate the experimental resolution. It is clear from figure 3 that the calculations for Co^{2+} in tetrahedral symmetry are in better agreement with the experimentally observed NEXAFS with $10Dq = -0.6$ eV. This optimum value of $10Dq$ is the same as reported by Wi *et al* [16]. In the literature various groups have reported different values of $10Dq$, such as -0.7 eV by Kobayashi *et al* [17] and -1 eV by Krishnamurthy *et al* [14]. The calculations performed for $10Dq = -0.7$ and -1.0 eV are also given in figure 3. The features around 777 and 779 eV are better reproduced for $10Dq = -0.6$ eV. With increase in the value of the crystal field energy, the features are shifting towards the higher energy side. From figure 3 it is clearly evident that the calculations better reproduce the L_3-edge as compared to the L_2-edge, but it is known that the L_3-edge is more sensitive to the local environment [15, 18]. The other common valence state of Co is 3+. Calculations performed for Co^{3+} (figures 3(i)–(l)) in the tetrahedral symmetry show a large spread as compared to the experimental spectra. Thus, it helps in excluding the Co^{3+} contributions in the present system. Based on these atomic multiplet calculations, it can be concluded that (1) there are no Co clusters present in the single-phase thin films, (2) Co is substituted at the Zn site in the ZnO matrix, (3) Co is present in 2+ charge state and (4) it is tetrahedrally surrounded by four O atoms with a crystal field splitting of -0.6 eV.

To further investigate the source of magnetism and the role of Co in the ZnO matrix, XMCD spectra were collected at the Co $L_{3,2}$-edge at 80 and 300 K for the CoZnO1 and CoZnO3 samples which are shown in figure 4. There is a small variation of the NEXAFS signal on the degree of polarization of the incident x-ray photon, but there is a reproducible difference between the NEXAFS collected for the photon helicity parallel and antiparallel with the applied magnetic field (0.3 T), which is the XMCD signal shown in figure 4. Further, it can be seen that there is no considerable

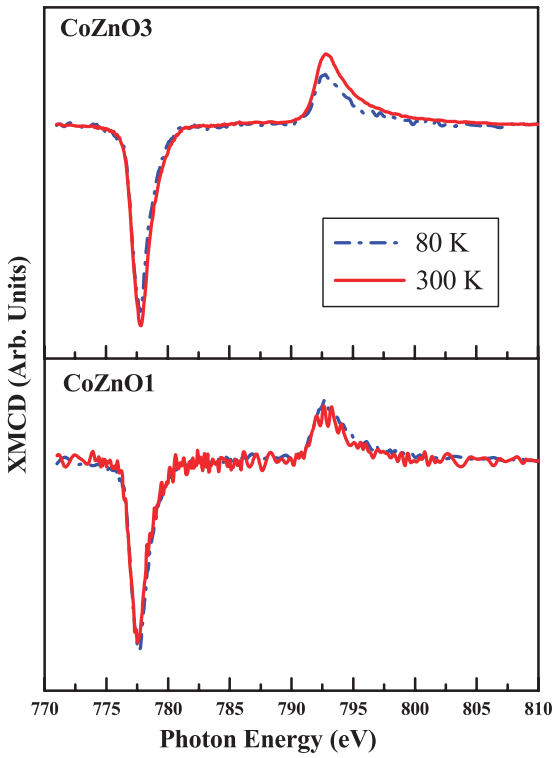

Figure 4. The XMCD spectra collected at the Co $L_{3,2}$-edge at 80 and 300 K of the CoZnO1 and CoZnO3 samples.
(This figure is in colour only in the electronic version)

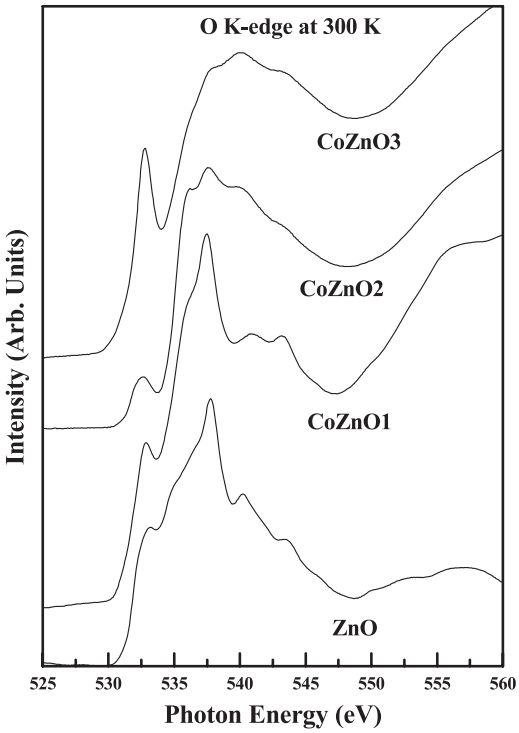

Figure 5. NEXAFS at the O K-edge collected at 300 K for the pure and Co doped ZnO thin films.

difference between the XMCD signal collected at 80 and 300 K. This temperature independence indicates that there is no paramagnetic contribution of the Co ions towards the magnetism of the system. Barla *et al* [19], in their Co doped ZnO samples, observed that the contribution of the Co sublattice was paramagnetic. The XMCD signal at the Co $L_{3,2}$-edge in their samples decreased with increasing temperature, but in our case there is almost no change in the XMCD signal with increasing temperature. Thus we can say that in our case the contribution of doped Co ions towards the magnetism in the system is ferromagnetic with almost no paramagnetic component. Sum rules were used to separate the spin and the orbital part of the magnetic contribution of Co using the following formulae:

$$\langle L_Z \rangle = \frac{2(A+B)}{3C} n_{\mathrm{h}}$$

$$\langle S_Z \rangle = \frac{(A-2B)}{2C} n_{\mathrm{h}}$$

where A and B are the areas under the L_3- and L_2-edge respectively for the XMCD curves, C is the area under the $L_{3,2}$-edge NEXAFS spectra and n_{h} is the number of holes in the 3d orbital of Co. Here we have neglected the magnetic dipole operator component. The errors introduced in the calculations due to this and other sources, as in the determination of background, rate of circular polarization and the number of electrons/holes in the 3d orbital are less than around 10%. It was confirmed from the experimental and calculated NEXAFS spectra that Co is in the 2+ state. Thus the number of holes in Co 3d states is taken to be three. The values of $\langle L_Z \rangle$ and $\langle S_Z \rangle$ so calculated for CoZnO1 are $0.084\mu_{\mathrm{B}}$ and $0.306\mu_{\mathrm{B}}$ at 80 K and $0.085\mu_{\mathrm{B}}$ and $0.239\mu_{\mathrm{B}}$ at 300 K, respectively. For the CoZnO3 sample the corresponding values are $0.029\mu_{\mathrm{B}}$ and $0.084\mu_{\mathrm{B}}$ at 80 K and $0.021\mu_{\mathrm{B}}$ and $0.116\mu_{\mathrm{B}}$ at 300 K, respectively. Thus with the change in temperature there is negligible change in the values of these components within an error of 10%. In the XMCD measurements performed by Milan Gacic *et al* [20], they found a large temperature dependence of the $\langle L_Z \rangle$ and $\langle S_Z \rangle$ values in their 5% Co doped ZnO thin films. In their case the corresponding values were $0.036\mu_{\mathrm{B}}$ and $0.141\mu_{\mathrm{B}}$ at 28 K and $0.008\mu_{\mathrm{B}}$ and $0.026\mu_{\mathrm{B}}$ at 300 K. They found both these values to be very close to the pure paramagnetic moment for Co^{2+}-ions. In our case these values are much higher, showing negligible temperature dependence. Thus the Co contribution to the magnetism in these systems is ferromagnetic. The magnetic moment per Co ion is less in the case of the CoZnO3 sample than in the CoZnO1 sample. These results are in good agreement with the magnetization results [11]. The orbital and the spin moments for the Co metal were determined to be $0.153\mu_{\mathrm{B}}$ and $1.55\mu_{\mathrm{B}}$ respectively by Chen *et al* [21]. These values are an order of magnitude different from the values in our samples. This further confirms that the magnetism in these samples is not due to the Co clusters and is due to the Co ion substituting Zn in the ZnO matrix.

O K-edge NEXAFS can be used to investigate the hybridization of the metal 3d orbitals with the host O 2p orbitals. The O K-edge arises mainly due to the transition of the O 1s electron to the conduction band near the Fermi surface, which is dominated by the O 2p and transition metal 3d

hybridized orbitals. O K-edge NEXAFS for pure ZnO thin film and for the CoZnO1, CoZnO2 and CoZnO3 samples are shown in figure 5 collected at 300 K. In the case of pure ZnO, the broad spectral features between 530 and 539 eV are assigned to the hybridization between the O 2p and the highly dispersive Zn 4s states, forming the bottom of the conduction band. The sharp peak at around 537 eV is due to the transition of O 1s electrons to more localized O $2p_z$ and $2p_{x+y}$ states [14]. The features between 539 and 547 eV are due to the transitions to the states formed due to the hybridization between the O 2p states with the Zn 4p states [23]. There are some systematic changes in the features of the O K-edge spectra with increase in Co doping. From figure 5 it is clear that with the increase in the doping concentration of Co in ZnO the intensity of the peak at around 532.5 eV is increasing. This may be due to the fact that with increase in the Co concentration more unoccupied 3d states are being introduced within the band gap of the ZnO which hybridize with the O 2p orbitals. Due to the increase in the density of unoccupied 3d states with Co doping, the intensity of this peak is increasing. Appearance of a similar peak with the Mn doping is also reported by Thakur *et al* [22] in their Mn doped ZnO samples. This assignment is in accordance with that of de Groot *et al* [23] and the calculations done by Yan *et al* [24]. However, this peak is also present in pure ZnO. It casts some doubt over this assignment of the peak. In the case of pure ZnO, Zn has $3d^{10}$ configuration. As no empty 3d states are available, so no pre-edge peak is expected. Thus this pre-edge peak, in the case of pure ZnO thin film, can also be due to some O vacancies or some other defects present in the system. At present this assignment is only speculative and more substantial arguments, based on the experiments, will be given later. The other notable change in the spectral features of the O K-edge with increase in Co doping is the decrease in the intensity of the peak at ∼537.5 eV and the broadening of the peaks with energy greater than around 538 eV. Such a broadening is also seen by Krishnamurthy *et al* [14] in their Co doped ZnO sample. They assigned this broadening to be due to the presence of the O vacancies and the Co doping. The presence of Co at the Zn site affects the O 2p states; due to the hybridization of Co 3d states with the O 2p states, the O 2p states are becoming more and more dispersive leading to the observed broadening of the spectral features with increasing Co content in the system.

Following various reports [7, 25] on the RTFM shown by many ZnO thin films having defects, it is important to investigate the magnetic contribution of defects (if any) that may be present in the ZnO thin films. If they are contributing to the magnetism in the system then this contribution needs to be considered to estimate the Co contribution in RTFM and to ascertain whether transition metal doping is at all necessary for the system to be ferromagnetic at room temperature. Thus controlled defects were introduced into the system by annealing the ZnO thin film in Ar atmosphere and implanting the ZnO thin films with 100 keV Ar-ions. Annealing in Ar atmosphere is supposed to increase the number of O vacancies whereas Ar-ion implantation can produce ion vacancies through head on collision with the target ions. Study of Ar-ion implanted thin films can also help in extracting

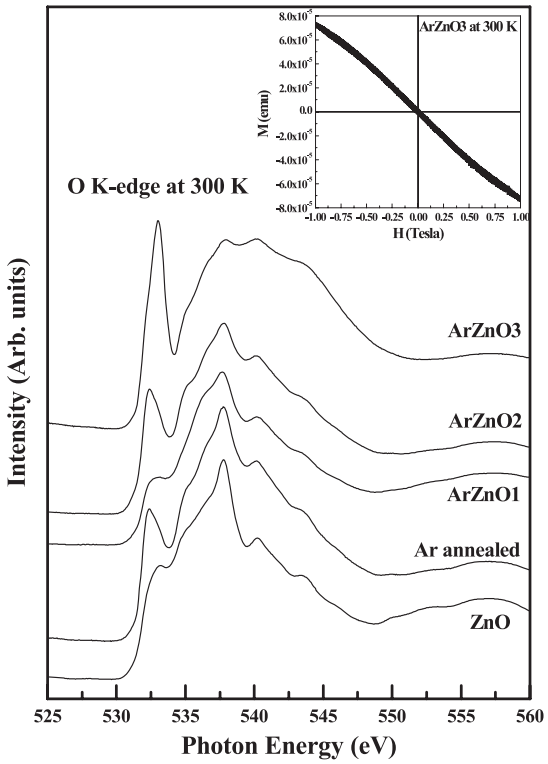

Figure 6. NEXAFS at the O K-edge collected at 300 K for the pure, Ar annealed and Ar-ion implanted ZnO thin films. The inset shows the M–H measurement done at 300 K for the ArZnO3 sample.

the magnetic contribution of implantation-induced defects which could have been introduced into the system during Co ion implantation. Isothermal magnetization hysteresis measurements performed at 300 K in these films confirmed no magnetic signal, except for the usual diamagnetic signal. The inset of figure 6 shows the isothermal magnetization hysteresis for the ArZnO3 sample at 300 K using AGFM. It shows diamagnetism with no indication of any ferromagnetic signal. This is contrary to the reports by Borges *et al* [7] where they have reported observation of RTFM in 100 keV Ar-ion implanted single crystals of ZnO. Thus the defect contribution towards the ferromagnetism shown by the system at room temperature is ruled out. Further effects of the defects introduced into the system by Ar annealing and Ar-ion implantation on the electronic structure of ZnO were studied with the help of O K-edge NEXAFS collected at 300 K, as shown in figure 6. It can be seen from figure 6 that the intensity of the pre-edge peak at around 532.5 eV is increasing with the increase in the number of defects in the system. There is a clear increase in the intensity of this peak after annealing in an Ar atmosphere. Also there is a considerable increase in the peak intensity with increase in implantation dose of the Ar-ion from 1×10^{16} to 1×10^{17} ions cm^{-2}. This pre-edge peak can be assigned to the O vacancies not to the structural disorder in ZnO, as this peak is present not only in the Ar-ion implanted samples but also in the Ar annealed sample. The consistent increase in the intensity of the pre-edge peak with Ar-ion implantation dose is an indication of the production of more defects with the increase in the ion implantation

dose. Similar to the case with Co doped samples, there is a broadening of features above 538 eV energies in the case of Ar-ion implanted samples with increase in implantation dose. Thus the broadening of the spectral features is due to the presence of the structural defects in the system. The decrease in the intensity of the peak at around 537 eV is an indication that due to the presence of defects in the system, the O $2p_z$ and $2p_{x+y}$ states are getting more dispersive. Based on this study of the Ar annealed and Ar-ion implanted samples it can be concluded that O vacancies play a major role in the appearance of pre-edge features in the metal doped ZnO, but the contribution from the hybridization of empty metal 3d states with O 2p states cannot be ruled out. Similarly, the broadening of features above the energy 538 eV may be due to the structural defects in the system and other defects, like Co present at the Zn site as an impurity.

4. Conclusions

In summary, thin films of ZnO are implanted with Co ions. The impurity phases/clusters present in the film just after implantation are successfully dissolved with the help of swift heavy ions, except for the sample implanted with an implantation dose of 1×10^{17} ions cm^{-2}. XRD measurements confirm the single-phase nature of the CoZnO1, CoZnO2 and CoZnO3 samples. However, no success is achieved in the case of the CoZnO4 sample which is due to the fact that the solubility limit of Co in ZnO has been crossed with this implantation dose. The NEXAFS at the Co $L_{3,2}$-edge shows the absence of Co clusters or other impurity phases in CoZnO1, CoZnO2 and CoZnO3 samples, as their spectral features are completely different from those of Co metal and other oxides of Co. The observed spectral features are due to the substitution of Co at the Zn site in the ZnO matrix and are supported by the atomic multiplet calculations for the Co ion tetrahedrally surrounded by four O atoms. The other information that is deduced from the calculations is that Co is present in the 2+ state and the crystal field splitting is −0.6 eV. The importance of Co doping is emphasized with the help of XMCD measurements performed on the system. It is suggested that the magnetism in this system is due to the Co substituting for Zn and not due to Co clusters. From the temperature independence of the XMCD spectra it is inferred that the contribution of Co is ferromagnetic, contrary to the report in the literature [19]. The NEXAFS spectra collected at the O K-edge give information regarding the role played by the defects in the electronic structure of ZnO. The appearance of a new peak at ∼532.5 eV and the broadening of the spectral features with increase in Co doping and Ar-ion implantation dose, is explained on the basis of the defects introduced into the system by doping and implantation. The presence of defects in the system overshadows the effects of the presence of Co at the Zn site in ZnO.

Acknowledgments

The authors are grateful to Dr Amit Roy, Director, IUAC, New Delhi for his keen interest in this work and the Pelletron group of IUAC for providing the swift heavy ion beam facility. Authors acknowledge the financial support from Department of Science and Technology (DST), India for this work under the project no. SR/S2/CMP/0051/2007.

References

[1] Awschalom D D and Flatté M E 2007 *Nat. Mater.* **3** 153
[2] Dietl T, Ohno H, Matsukura F, Cibert J and Ferrand D 2000 *Science* **287** 1019
[3] Naeem M, Hasanain S K and Mumtaz A 2008 *J. Phys.: Condens. Matter* **20** 025210
[4] Coey J M D, Venkatesan M and Fitzgerald C B 2005 *Nat. Mater.* **4** 173
[5] Potzger K, Zhou S, Grenzer J, Helm M and Fassbender J 2008 *Appl. Phys. Lett.* **92** 182504
[6] Pan H, Yi J B, Shen L, Wu R Q, Yang J H, Lin J Y, Feng Y P, Ding J, Van L H and Yin J H 2007 *Phys. Rev. Lett.* **99** 127201
[7] Borges R P, da Silva R C, Magalhães S, Cruz M M and Godinho M 2007 *J. Phys: Condens. Matter* **19** 476207
[8] Thole B T, Carra P, Sette F and van der Laan G 1992 *Phys. Rev. Lett.* **68** 1943
[9] Carra P, Thole B T, Altarelli M and Wang X 1993 *Phys. Rev. Lett.* **70** 694
[10] Angadi B, Jung Y S, Choi W K, Kumar R, Jeong K, Shin S W, Lee J H, Song J H, Wasi Khan M and Srivastava J P 2006 *Appl. Phys. Lett.* **88** 142502
[11] Kumar R, Singh F, Angadi B, Choi J W, Choi W K, Jeong K, Song J H, Wasi Khan M, Srivastava J P and Tandon R P 2006 *J. Appl. Phys.* **100** 113708
[12] Jung Y S, Kononenko O, Kim J S and Choi W K 2005 *J. Cryst. Growth* **214** 418
[13] Wang Z G, Dufour Ch, Paumier E and Toulemonde M 1994 *J. Phys.: Condens. Matter* **6** 6733
[14] Krishnamurthy S *et al* 2006 *J. Appl. Phys.* **99** 08M111
[15] de Groot F M F, Abbate M, van Elp J, Sawatzky G A, Ma Y J, Chen C T and Sette F 1993 *J. Phys.: Condens. Matter* **5** 2277
[16] Wi S C *et al* 2004 *Appl. Phys. Lett.* **84** 4233
[17] Kobayashi M *et al* 2005 *Phys. Rev.* B **72** 201201 (R)
[18] van der Laan G and Kirkman I W 1992 *J. Phys.: Condens. Matter* **4** 4189
[19] Barla A *et al* 2007 *Phys. Rev.* B **76** 125201
[20] Gacic M, Jakob G, Herbort C, Adrian H, Tietze T, Brück S and Goering E 2007 *Phys. Rev.* B **75** 205206
[21] Chen C T, Idzerda Y U, Lin H-J, Smith N V, Meigs G, Chaban E, Ho G H, Pellegrin E and Sette F 1995 *Phys. Rev. Lett.* **75** 152
[22] Thakur P, Chae K H, Kim J–Y, Subramanian M, Jayavel R and Asokan K 2007 *Appl. Phys. Lett.* **91** 162503
[23] de Groot F M F, Grioni M, Fuggle J C, Ghijsen J, Sawatzky G A and Petersen H 1989 *Phys. Rev.* B **40** 5715
[24] Yan W, Sun Z, Liu Q, Li Z, Pan Z, Wang J, Wei S, Wang D, Zhou Y and Zhang X 2007 *Appl. Phys. Lett.* **91** 062113
[25] Xu Q *et al* 2008 *Appl. Phys. Lett.* **92** 082508